Chapter 4 – Design of Vector Magnetic Field Sensor System

4.1 3-Dimensional Vector Field Representation

The vector magnetic field is represented as a combination of three components along the Cartesian coordinate axes. The field along each of the three axes can be individually measured by sensors placed in the direction of the corresponding component. A single sensor can be easily used to measure the amplitude and direction of the magnetic field in that direction. The amplitude of the component is directly represented by change in the sensor output voltage and the direction can be obtained by comparing the output voltage with the reference voltage (output at the initial operating point). Thus the change in voltage is positive or negative depending on the direction of the applied magnetic field.

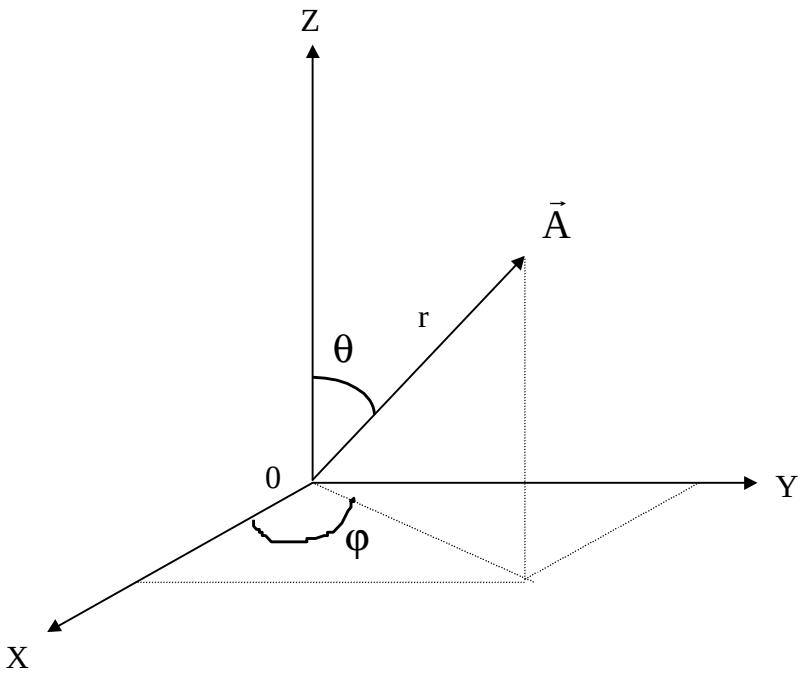

Figure 4.1 Vector representation of magnetic field.

The vector $\vec{A}$ can be expressed as

$$\vec{A} = A_x \hat{x} + A_y \hat{y} + A_z \hat{z} \quad \text{(Cartesian coordinates)} \tag{4.1}$$

where $A_x = r.sin\theta.cos\varphi, A_y = r.sin\theta.sin\varphi, A_z = r.cos\theta$. The vector field can also be represented in spherical coordinates as shown in Figure 4.1 by using Equations (4.2), (4.3) and (4.4). Hence in spherical coordinates

$$r = \sqrt{A_x{}^2 + A_y{}^2 + A_z{}^2}\ , \tag{4.2}$$

$$\theta = tan^{-1}\left(\sqrt{\frac{A_x{}^2 + A_y{}^2}{A_z{}^2}}\right), \tag{4.3}$$

$$\varphi = tan^{-1}\left(\frac{A_y}{A_x}\right). \tag{4.4}$$

Thus the amplitude and direction of the vector magnetic field can be calculated if the three Cartesian components of the field are known. The arrangement of the sensors for measuring these three components is as shown in Figure 4.2. Figure 4.3 shows the initial operating point of each of the sensors. As can be seen from the figure, the movement of the operating point along the slope depends on the overall applied magnetic field and can thus be used to measure both the amplitude and direction of the applied field.

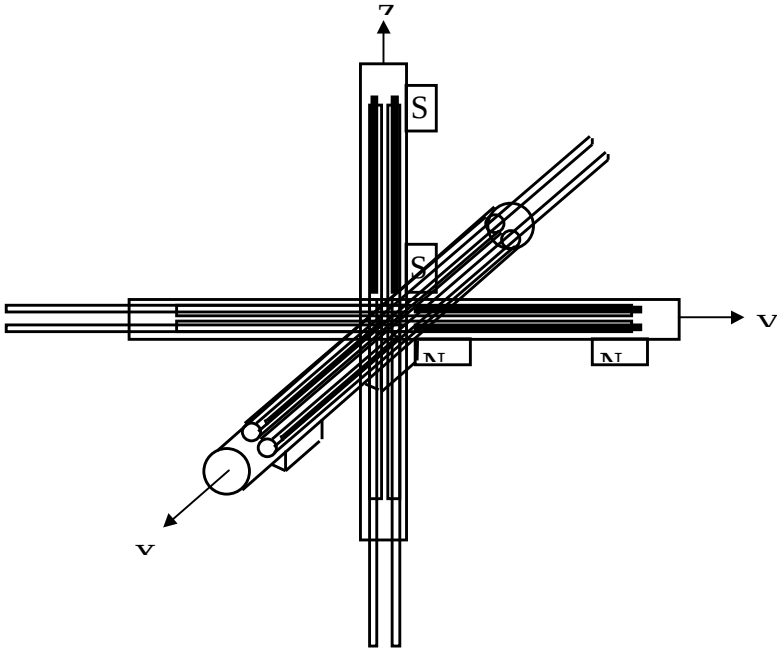

Figure 4.2 Sensor arrangement.

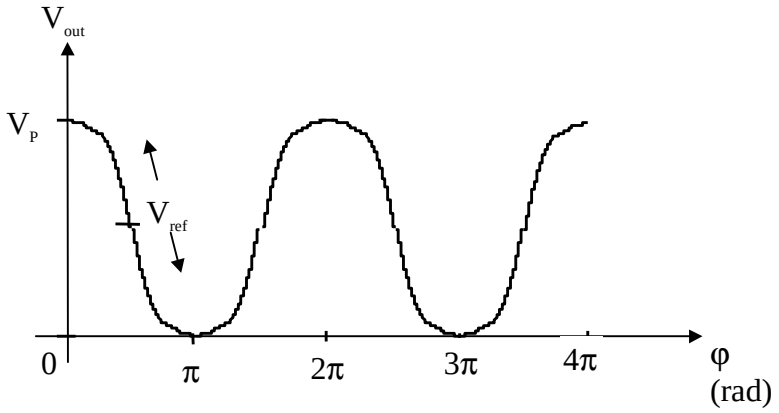

Figure 4.3 Initial operating point of the sensors.

If the direction of the external applied magnetic field is opposite to that of the biasing field, the overall magnetic field applied to the sensor decreases and so does the length of the Metglas wire. Thus the phase difference between the first and second reflection increases. If the sensor operates at the point shown in Fig. 4.3, the output voltage falls below the reference voltage. In

this case the direction is same as that of the biasing field, the output voltage goes above the reference voltage. Thus the direction of the applied magnetic field can be easily determined.

4.2 Design of Vector Field Measurement System

4.2.1 Sensor Head Design

In order to avoid magnetic induction in the sensor head, the material for sensor packaging should be ferrimagnetic. Aluminum is one likely candidate. It also has the advantage of light weight and large heat capacity. Figure 5.3 shows a schematic view of the sensor head. The circular hole, bored in each of the rectangular projections of the sensor head, houses the two quadrature phase shifted sensors used to measure the field in that particular direction. The small biasing magnets are also housed in the holes along with the sensors. The sensor head itself is machined from a solid block of aluminum in order to enhance the mechanical stability of the sensor elements.

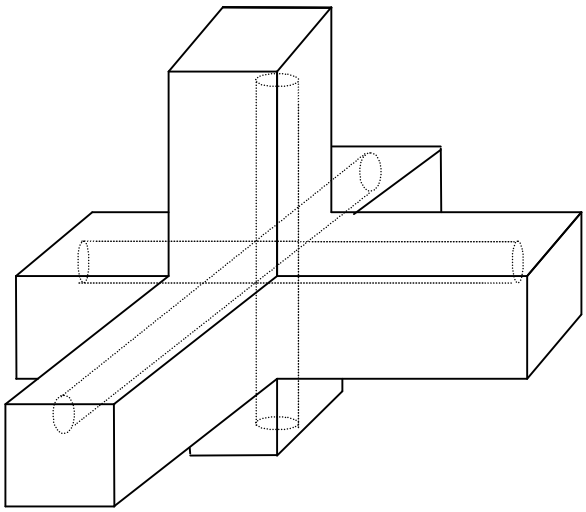

Figure 4.4 Sensor head for vector magnetic field measurement.

4.2.2 System Design with 3 Separate Laser Sources

In this design, each sensor pair has its own laser diode source. Figure 4.5 shows the schematic for this particular design.

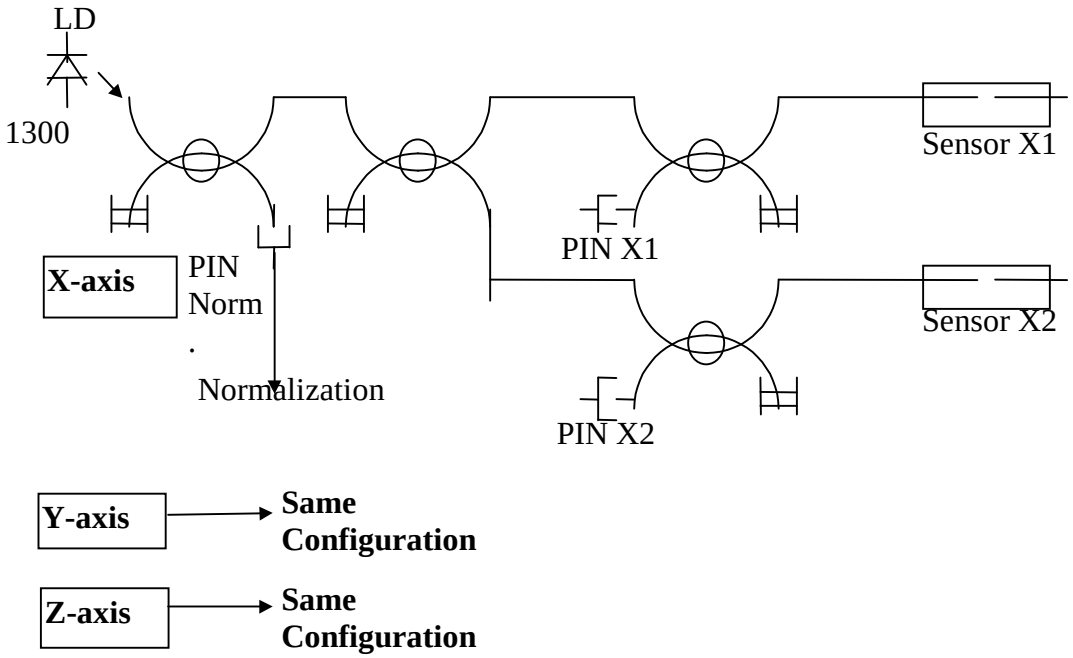

Figure 4.5 Design using three separate laser diodes.

Each laser diode has to drive at least three channels. Two for the quadrature phase shifted sensors themselves and one for the normalizing input. Thus the design consists of three stages of 3-dB couplers. The optical power at the input of the PIN diodes is thus 12 dB below the output of the laser diode in addition to the optical power loss at the sensor element. The advantage of using this design is the possibility of using low-power laser diodes for each axis and enhanced total system reliability. The disadvantage is cost.

4.2.3 System Design with Single Laser Source

Figure 4.6 shows the schematic for this design. In this particular design, only a single channel is needed for the normalization input. Thus the total minimum number of channels required is seven. The design has four stages of 3-dB fiber couplers introducing an attenuation of 15 dB at the input of the PIN diode. Thus in this case, higher power laser diode is certainly required.

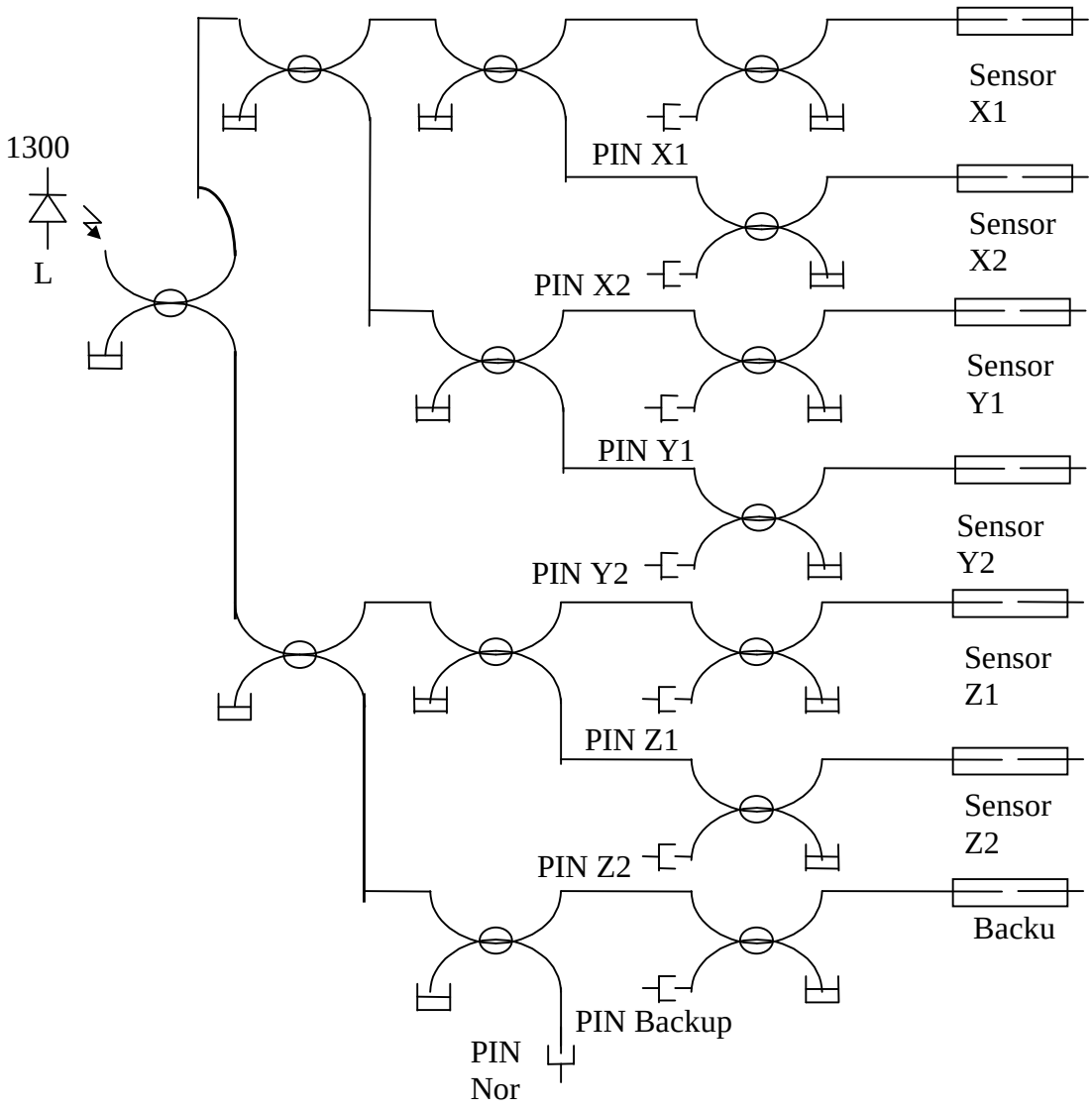

Figure 4.6 Design using single laser diode.

Table 4.1 shown below compares the resource requirements and advantages/disadvantages of the two designs.

Table 4.1 Resource comparison for three-diode and single-diode designs.

	Three-diode design	**Single-diode design**
Total channels	9(6+3)	8(7+1)
PIN Diodes	9	8
3-dB couplers	12	14
Temperature controllers	3	1
Current drivers	3	1
Remarks	Lower laser-diode power, large number of supporting components, three normalizations, costly.	Less components, slightly higher laser-diode power, less number of supporting components, single normalization, reliable, less costly.

4.2.4 Channel Amplifier Design

The output of the sensor has to be converted into an electrical form before it can be used for further signal demodulation. Fig. 6 shows the schematic of the circuit diagram used for this purpose. The light returning from the sensor is coupled to the PIN diode operated in reverse bias. The current flowing through the diode is directly proportional to the intensity of the returning light. A low-input bias current operational amplifier (OP Amp) is used as an I-to-V converter in the first stage of the circuit. The gain of this stage can be adjusted to any value, by simply changing the value of the resistance in the feedback loop. The second stage of the circuit is a simple subtractor for eliminating the offset in the output of the sensor. The final stage is a voltage follower with high input impedance to prevent loading of the previous stage.

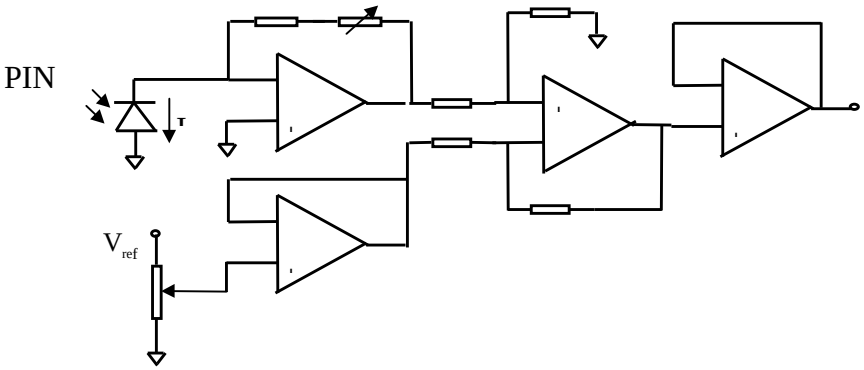

Figure 4.7 Preamplifier circuitry for a single channel.

4.3 Microprocessor-based Signal Demodulation and Processing

The signal processing system in the optical fiber based magnetometer consists of the opto-electronic part, the signal demodulation part and the display. The opto-electronic part converts the optical signal output from the sensors into electrical form and the quadrature phase shift (QPS) signal demodulation part obtains phase information from it. After the calibration the output is displayed in terms of external magnetic flux density measured. Figure 4.8 shows the schematic of the signal processing involved in the magnetometer system.

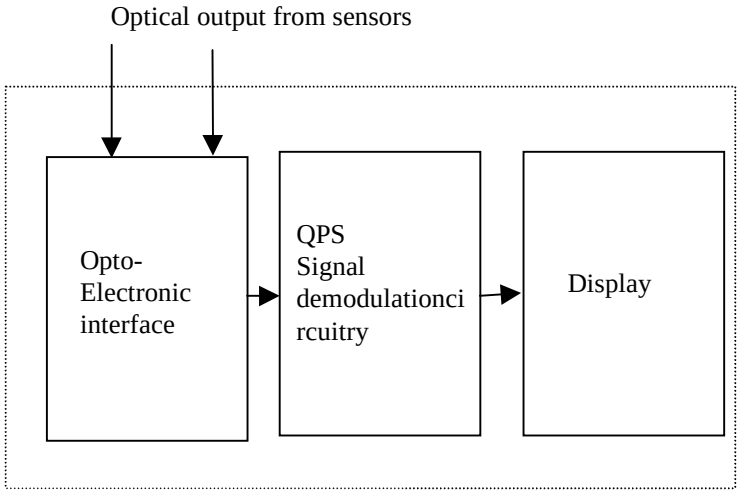

Figure 4.8 Components of the electronic signal processing system.

After the sensor output is converted into electrical form, Quadrature Phase Shift (QPS) signal demodulation scheme is applied in order to detect the phase signal. This technique ensures the signal phase detection regardless of the initial phase of the sensor. Each sensor can be brought to its initial operating point to obtain quadrature relationship by adjusting the initial air gap. A basic block diagram of the signal demodulation system for a single axis is shown in Figure 4.9.

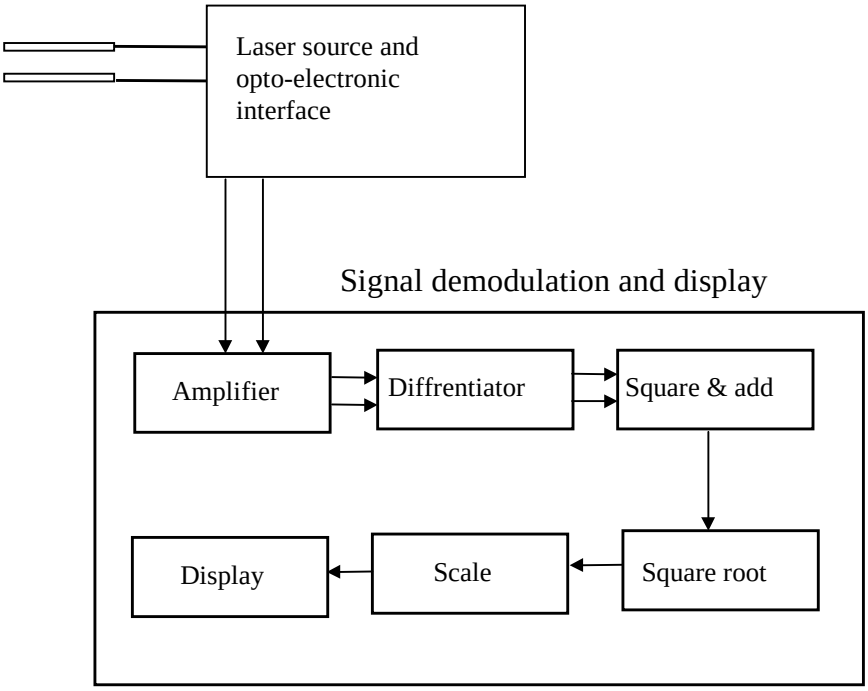

Figure 4.9 Block diagram of QPS signal demodulation scheme.

The signal demodulation scheme can be implemented in either analog or digital circuitry. The analog implementation of the scheme was discussed in the previous chapter in detail. The analog system implementation is simple in design and fabrication, but it shows several major disadvantages. Additional thermal noise generated in the calculation circuit degrades the SNR of the overall system. The components like resistors and capacitors, with precise values for calculation, are generally not easily available. The linear integrated circuits like multipliers and dividers have inherent inaccuracy in the computed signal output. The fabrication of the circuit and revision are time consuming. Since SNR, accuracy, flexibility and speed are required in the high sensitivity magnetometer system, the analog implementation of the signal

demodulation could be avoided for this particular application. Hence a microprocessor-based, digital signal demodulation scheme is implemented in the 3 dimensional magnetic field measuring system.

A microprocessor based signal demodulation scheme is used in the final magnetometer system. This increases the signal processing accuracy as well as increases system reliability and flexibility. The schematic of the digital implementation is shown in Figure 4.10.

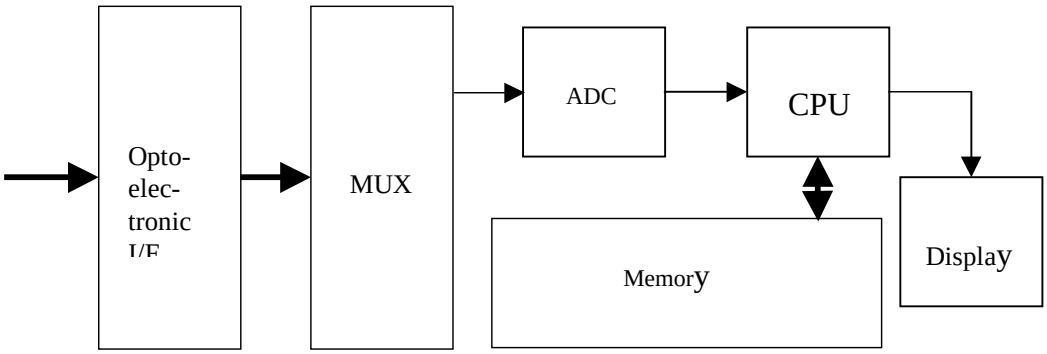

Figure 4.10 Block diagram of microprocessor-based signal demodulation system.

The electrical signals from the sensors and the normalizing input from the laser source are supplied into the 16X1 multiplexer from the opto-electronic interface. The analog to digital converter (ADC) converts each electric signal into a 12 bit word. The central processing unit (CPU) does all the calculations like normalizing, differentiating, squaring and adding on this data and displays the results on a LCD panel. The software instructions for the signal processing are stored in the flash memory and can be directly accessed by the microprocessor. Intel's 386EX CPU with a clock speed of 25 MHz based single board computer (SBC) was chosen for this application. The output from the three pairs of sensors and the normalizing input are supplied to the SBC through a 16 channel, 12-bit ADC with an input range of 0-10 V. Hence the resolution of the ADC is around 2 mV. The sampling rate can be as high as 100 kHz. Once the input data is converted into digital form, all the calculations required for quadrature phase shift demodulation are done in digital domain. Then the output is displayed

on a 4X20 character LCD panel. The operation of the SBC can be modified whenever required by downloading new executable files from a PC through a serial port and RS232 cable. This factor gives much higher operational flexibility as compared to analog signal demodulation circuitry. There are several advantages of the microprocessor-based signal demodulation. The thermal noise can be reduced significantly as output of preamplifier is directly converted to digital format without further analog processing. The system reliability is increased as commercially available single board computer is used for the signal demodulation scheme and sufficient resolution for the required application is ensured. The efficiency of operation is enhanced since this simply involves modification of software.

4.4 Fabricated Vector Field Measuring System

Figures 4.11 through 4.14 show the complete, fabricated optic-fiber based magnetometer system.

Figure 4.11 Experimental arrangement of magnetometer system.

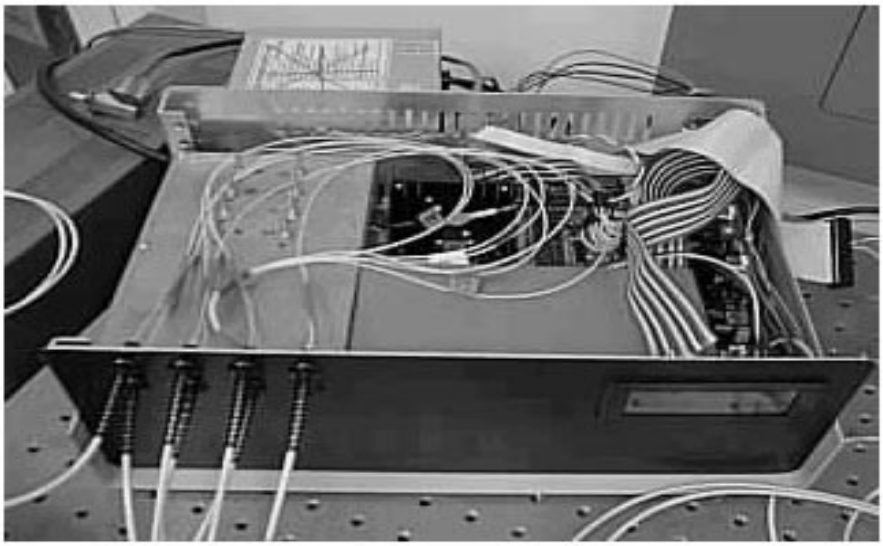

Figure 4.12 Electronic signal processing system box.

Figure 4.13 Calibration setup.

Figure 4.14 Complete experimental setup.

4.5 System Calibration

4.5.1 Experimental Setup

The sensors are packed in a V-groove aluminum bar and small capillary tubes as shown in Figure 4.15. Since the phase variation of each sensor on application of external magnetic field depends on a variety of factors, it is essential to calibrate each axis independently. The voltage output of each sensor primarily depends on its operating point, fringe visibility and the strain induced in it due to bending of the fiber.

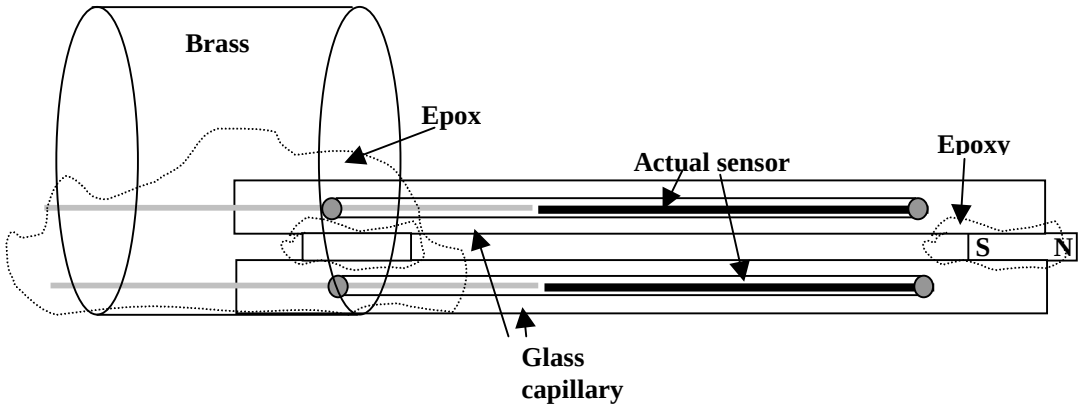

Figure 4.15 Schematic of a single axis sensor assembly.

As shown in the figure, each individual sensor consists of an EFPI involving a magnetostrictive wire with about a diameter of 125 μm. The wire is field-annealed and polished at an angle to increase the fringe visibility of the sensor output. Both the fiber and the sensing wire are enclosed in a borosilicate glass tube with an ID of about 150 μm. The tube is sealed at both ends using epoxy. Each sensor is then sealed inside a glass capillary tube. Two such sensors, which are in quadrature, are then glued together along with two permanent magnets for DC bias using epoxy. The quadrature phase shifted sensor pair is then attached to the inner surface of a small length of brass tube. This reduces the bending-induced strain on the sensors as well as facilitates the insertion of the assembly into the aluminum sensor support.

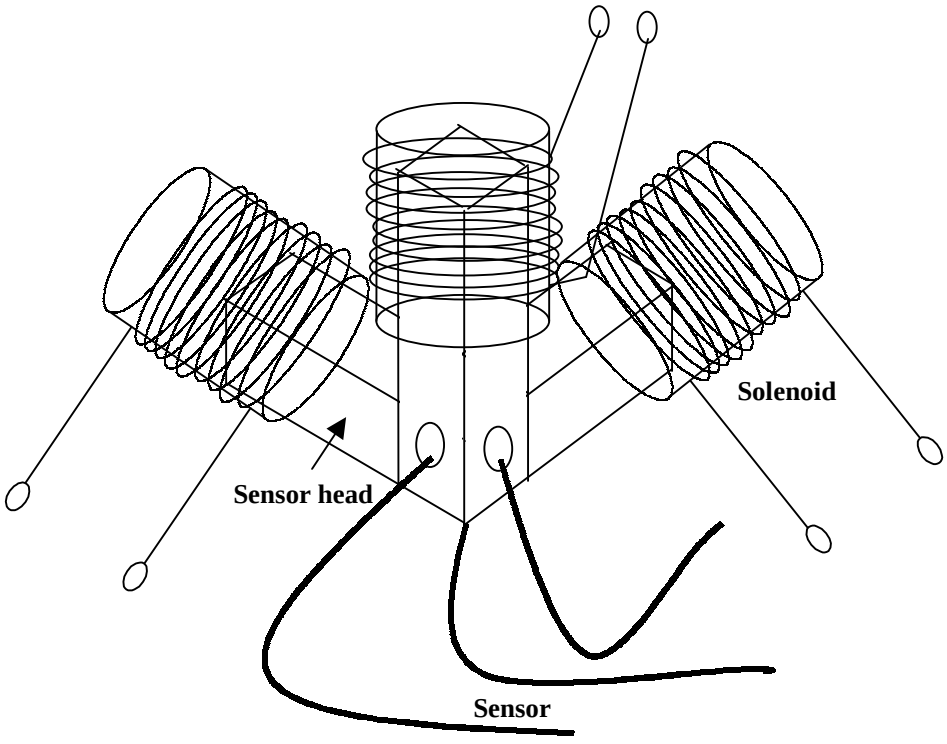

Figure 4.16 Experimental setup.

Figure 4.16 shows the overall experimental setup. The quadrature phase shifted, DC field biased sensor pairs are inserted in the cylindrical holes along the three axes of the aluminum sensor head. Each arm of the sensor head is placed in a solenoid capable of producing the necessary

calibration flux density. The first part of the experimental procedure deals with determining the magnetic field response of each of the individual sensors. In the second part, the microprocessor-based signal demodulation system calculates the overall signal for each axis. This is essentially the calibration procedure to determine the relation between the calculated output and the applied external magnetic field. The signal demodulation system samples each sensor output at a rate of 18 Hz. The digitized signal is then averaged over two seconds, normalized to the laser source variation and then used in further calculations. The following sections describe the calibration procedure and the obtained results in detail.

4.5.2 Calibration Procedures

In order to determine the magnetic field response of each sensor, the sensor pair under investigation was placed inside the calibration coil. The operating point of the sensor with respect to its peak to peak value was observed. A DC magnetic field was then applied and varied in steps from – 40,000 nT to 40,000 nT. The voltage output of each sensor versus the applied magnetic fields was observed and measured using an oscilloscope or voltmeter because measured voltage values should be converted to magnetic flux after the calibration when using single-board computer as the calculation system. The calibration curve is loaded to the EEPROM in single-board computer board after this stage calibration is done. The procedure was repeated one more time and similar reading were obtained. The magnetic field response (low and high field) for each sensor was plotted. These results are presented in the next section.

4.5.3 Experimental Results

The plots showing the results of the experiments described above are presented below. Figures 4.17 (a) and (b) show the low and high field response of sensor 3 respectively. As can be seen from the figures, the low field response is more linear than the high field response. This is because although the sensor operates in the linear range of the fringe at lower field strengths, at

higher fields the operation enters into the nonlinear region of the fringe. This means that the phase difference of two sensors are not exactly 90 ^{o}. This effect is more clearly visible in some of the plots presented later.

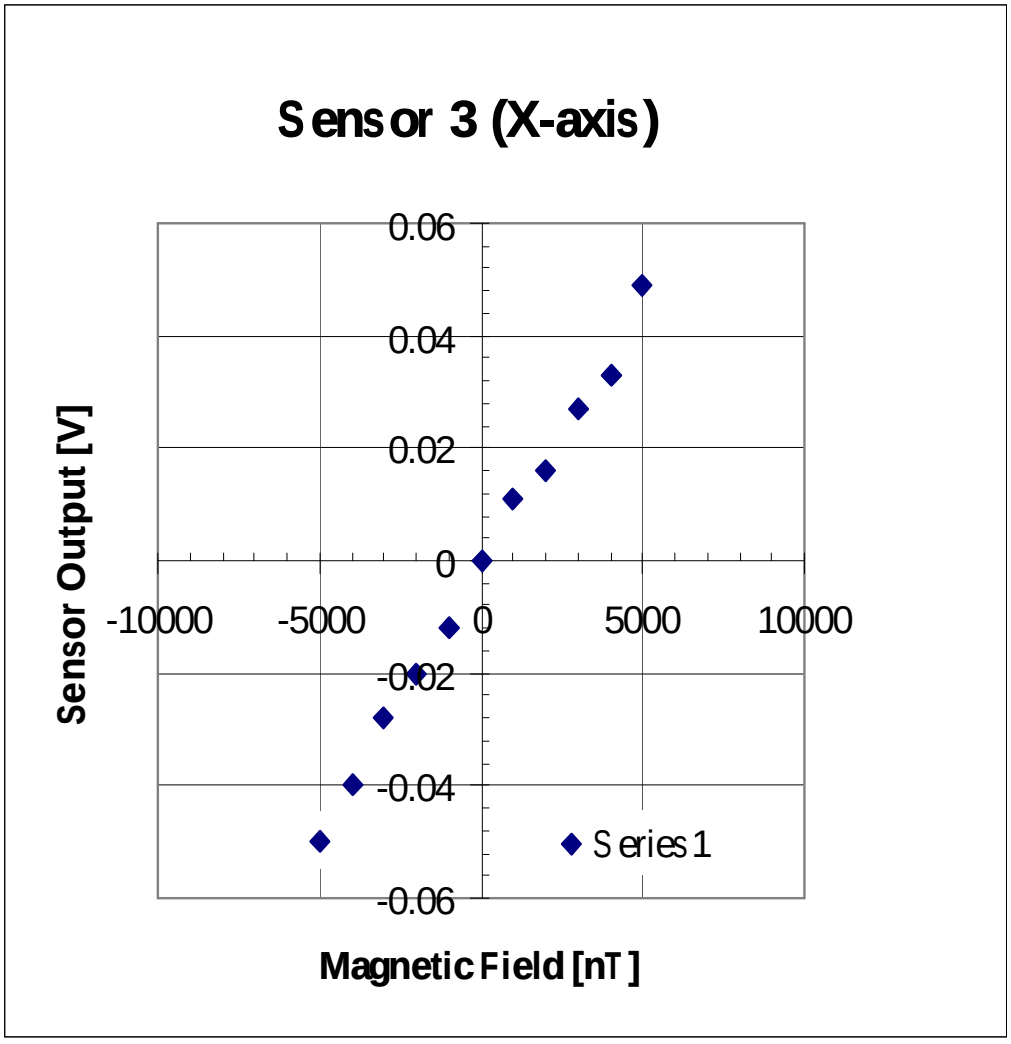

Figure 4.17 (a) Low field response of sensor 3 (X-axis).

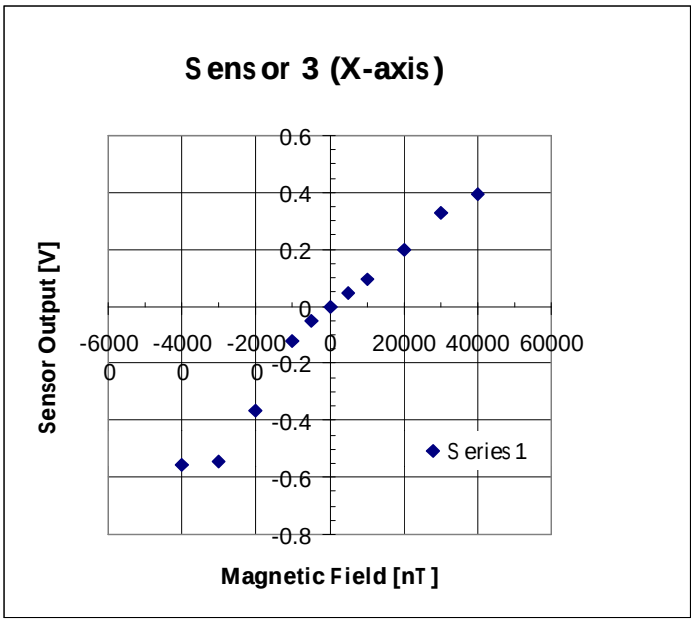

Figure 4.17 (b) High field response of sensor 3 (X-axis).

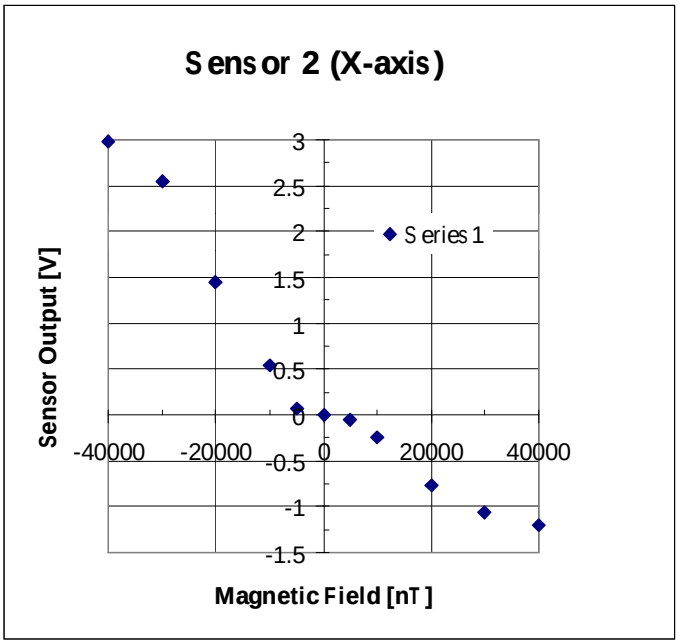

Figure 4.18 Field response of sensor 2 (X-axis).

As can be seen in Figure 4.18, sensor 2 does not show a good low field response. It operates either near the top or the bottom of the fringe and hence shows low sensitivity. The plot also indicates that the operating point is not exactly at the bottom or top. If this were the case, the output voltage variation on application of positive and negative magnetic fields would be in the same direction. Figures 4.19 (a) and (b) show the magnetic field response of sensor 4. As from the figures, the response is exactly opposite to that shown by sensor 3. The direction of voltage variation depends not only on the operating point along the fringe but also on the slope of operation. Sensor 4, though operating near the center (as can be seen from the linear low-field response), operates on the other side of the fringe (similar to sensor 2) and hence shows an output variation exactly opposite of that shown by sensor 3.

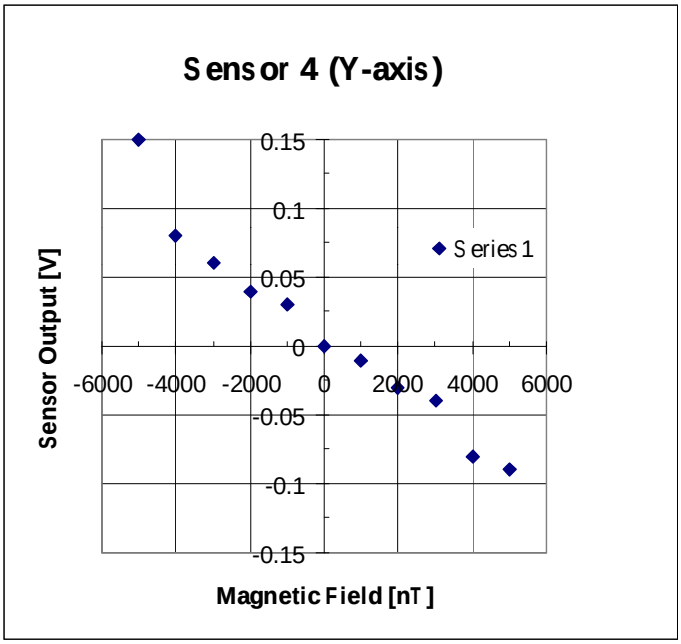

Figure 4.19 (a) Low field response of sensor 4 (Y-axis).

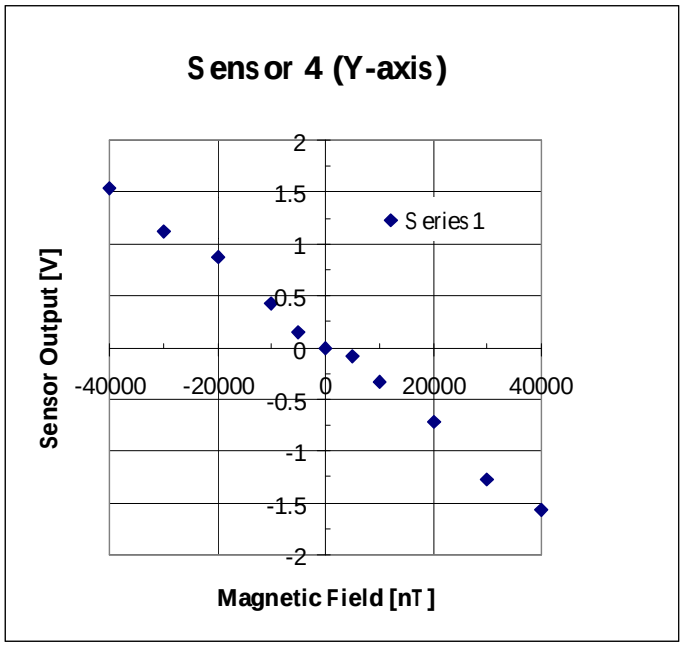

Figure 4.19 (b) High field response of sensor 4 (Y-axis).

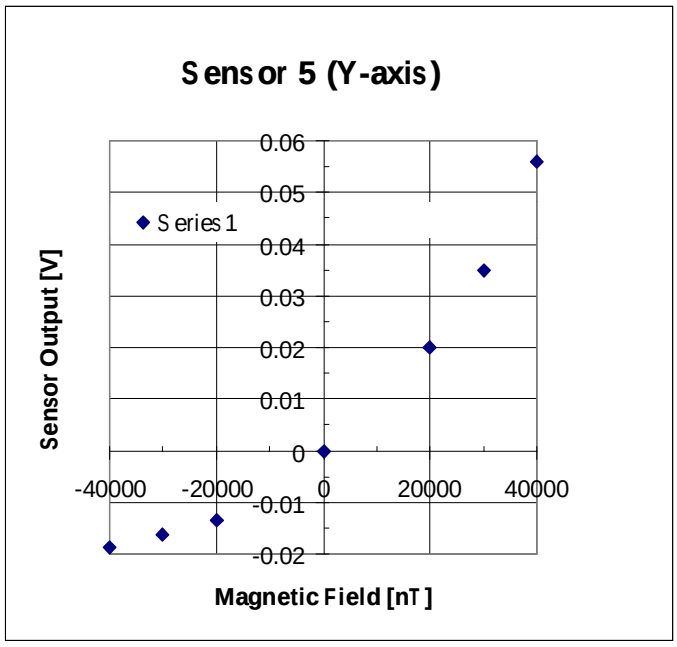

Figure 4.20 Field response of sensor 5 (Y-axis).

As seen in Figures 4.20, sensor 5 exhibits a response similar to that shown by sensor 2. It operates either near the bottom or the top of the fringe and hence shows low sensitivity. Like sensor 2, the operating point of sensor 5 is not exactly at the peak. However the slope of operation is similar to that of sensor 3. Figures 4.21 (a) and (b), and Figure 4.22 show the low and high field response of sensors 6 and 7 respectively. As can be seen from the figures, both the sensors show visibly non-linear response even for low fields. The sensors, since slightly not in quadrature with each other, operate near the top and bottom of the fringe and thus in the non-linear region of operation.

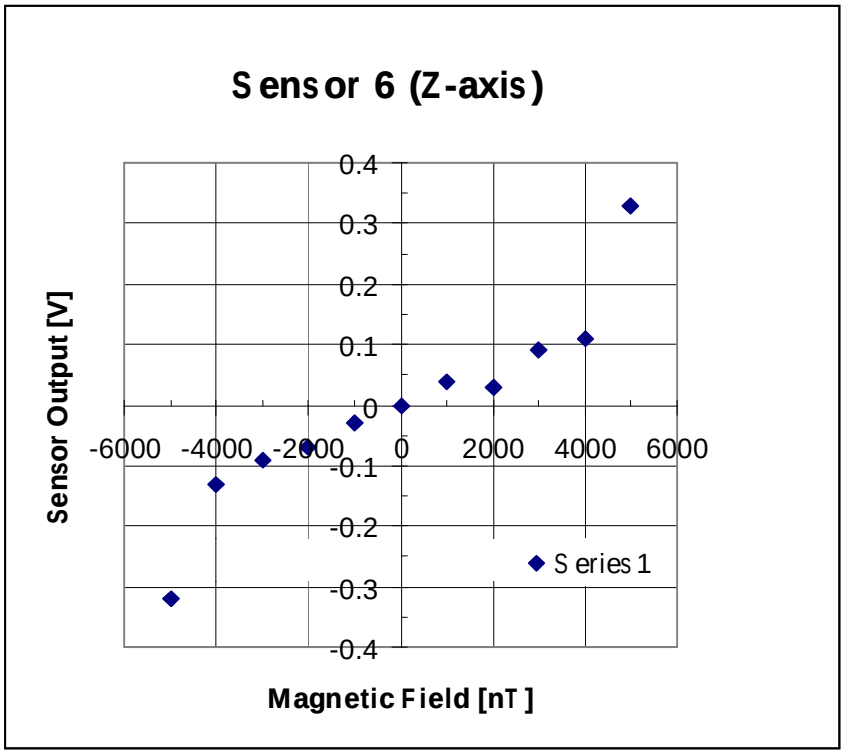

Figure 4.21 (a) Low field response of sensor 6 (Z-axis).

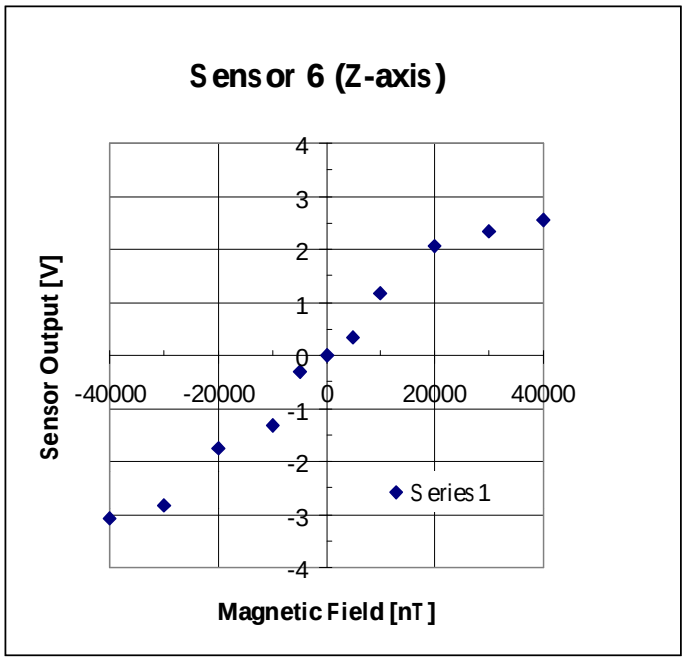

Figure 4.21 (b) High field response of sensor 6 (Z-axis).

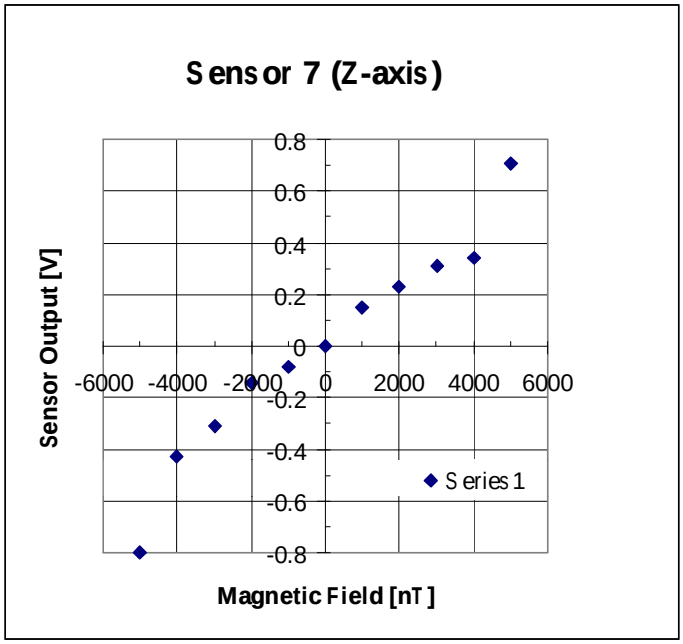

Figure 4.22 Low field response of sensor 7 (Z-axis).

Figures. 4.23, 4.24 and 4.25 show the calibration curves for the X, Y and Z axes of the magnetometer system. The figures show the output calculated by the signal demodulation system, plotted against the applied external magnetic field. All the calibration curves exhibit a certain level of non-linearity which can be attributed to the non-uniform response of the individual sensors to the same external applied field

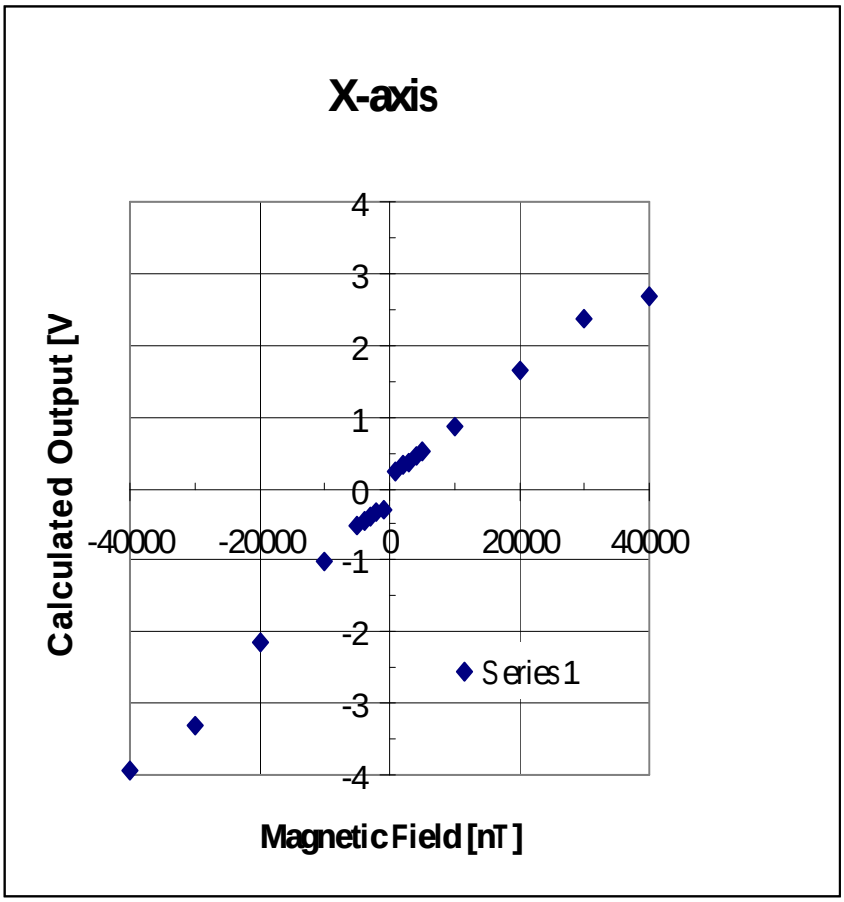

Figure 4.23 Calibration curve for X-axis.

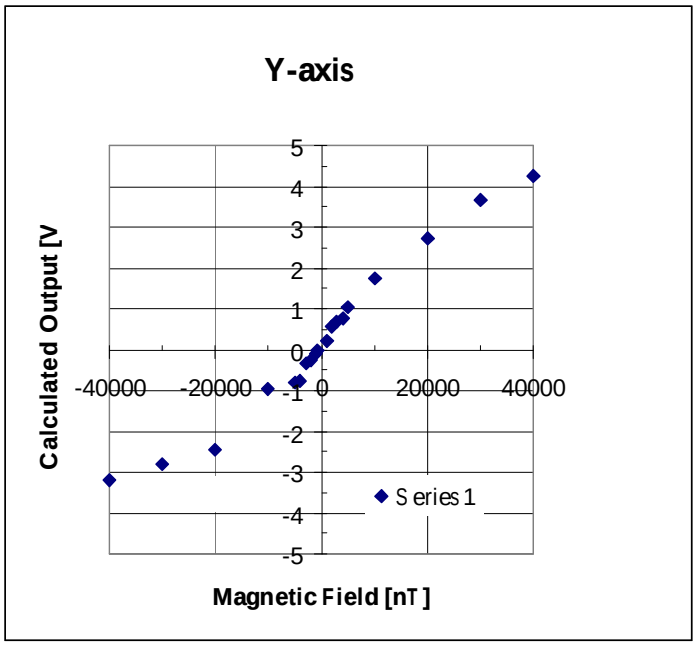

Figure 4.24 Calibration curve for Y-axis.

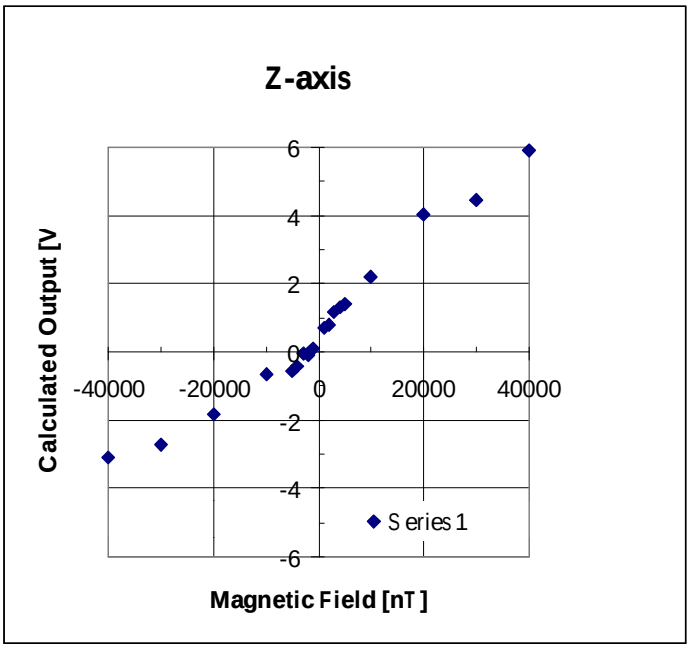

Figure 4.25 Calibration curve for Z-axis.

The calibration curve for sensor system output after signal demodulation is given in Figure 4.26 to Figure 4.28. The first rows of Figures 4.26 to 4.28 show the system response with applying calibration magnetic field applied from –40,000 to +40,000 nT. The outputs are voltages for input to the digital signal demodulation circuitry. After having system voltage outputs, the polynomial curve fitting is performed in order to convert sensor system output voltage into measured magnetic flux density which are presented in LCD panel. The 'O' and '*' are curve fitted points and original data points for system output respectively. A 4th order polynomial fit is done in this experiment and the coefficients of the fitted curve are reinserted signal demodulation program so that final reading on LCD panel is magnetic flux density (nT) directly. Since the given earth magnetic field, the components of the field affects the total magnetic field variation.

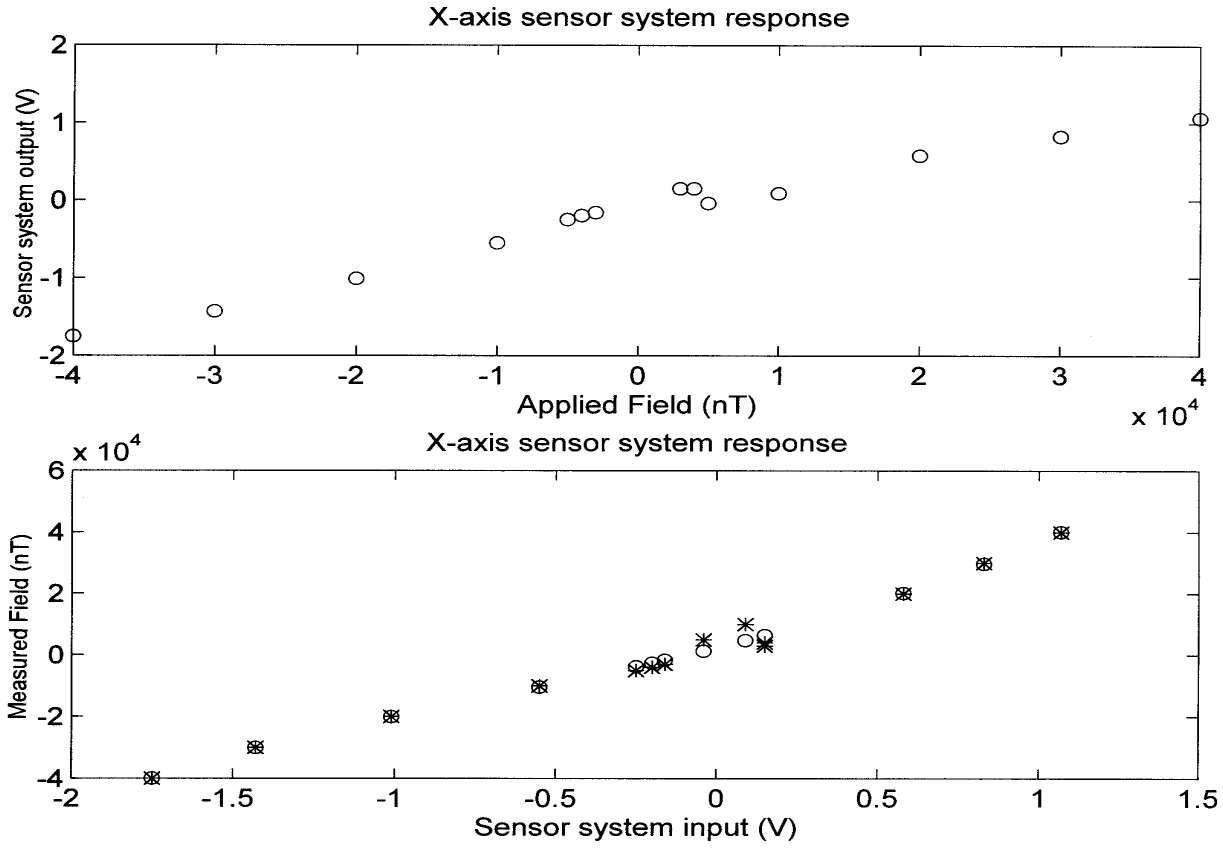

Figure 4.26 X-axis system response.

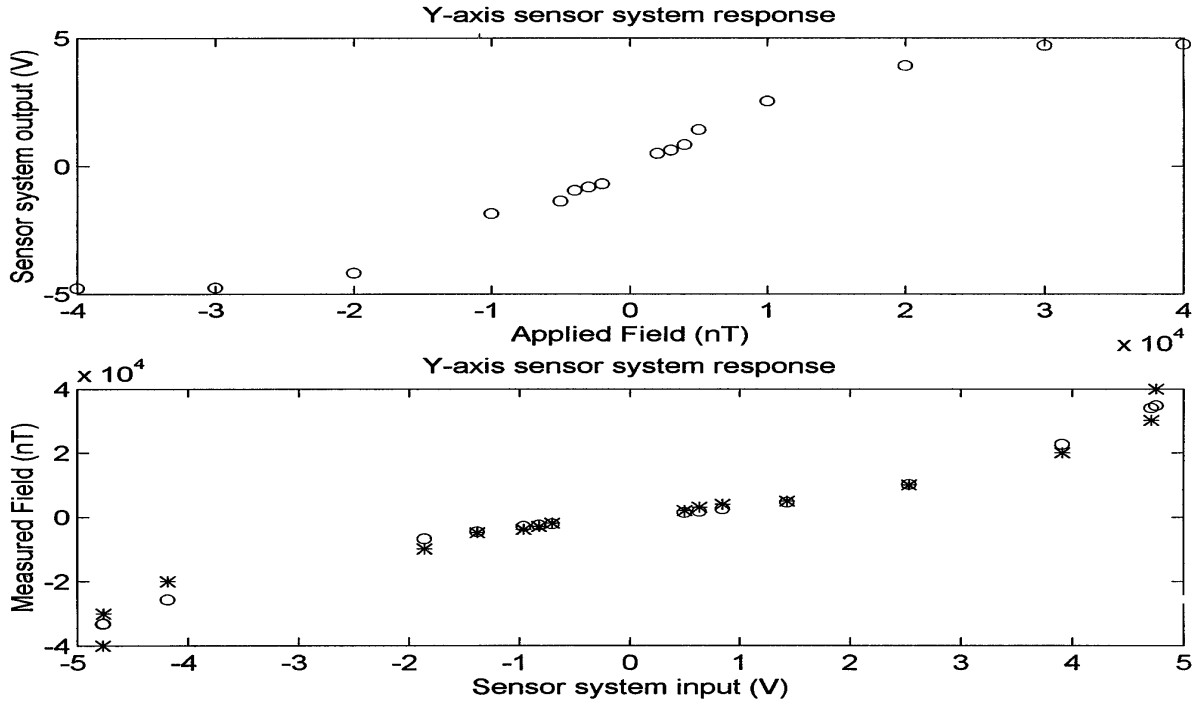

Figure 4.27 Y-axis system response.

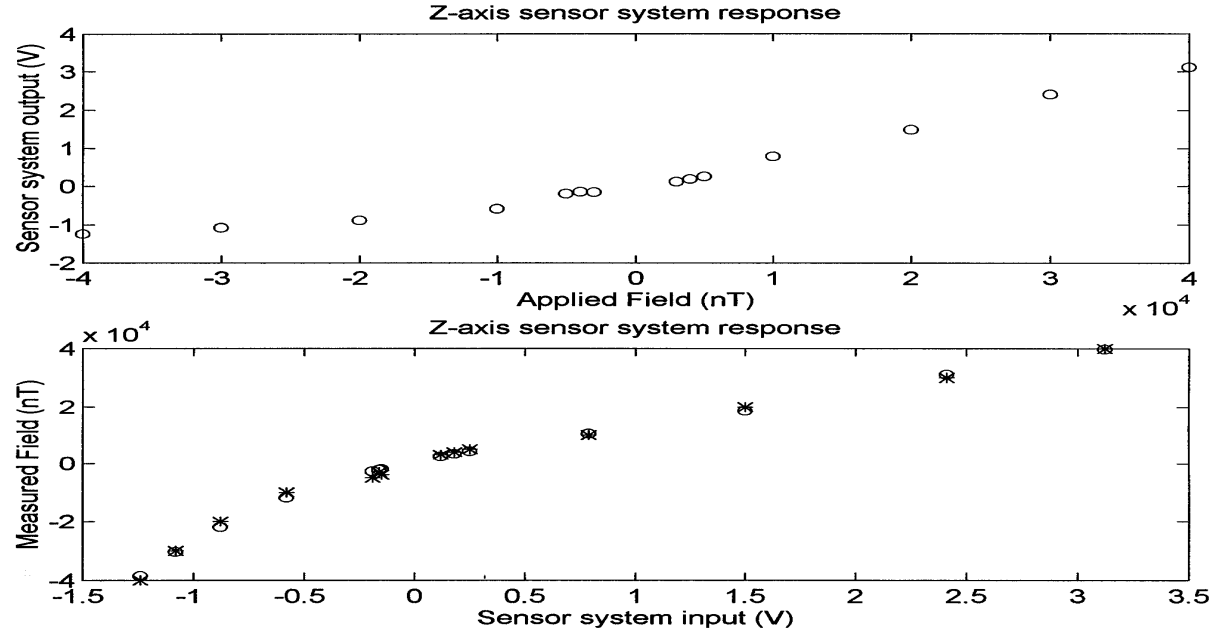

Figure 4.28 Z-axis system response.

After finishing the first calibration which allows to measure sensor output voltages corresponding applied magnetic field, a second stage calibration is performed to represent measured magnetic field on the display in the microprocessor based signal demodulation system. In the second stage calibration, the value of each axis for applied field and sensor output voltage is converted as an inverse function, i.e., in Figure 4.28, x-axis (magnetic flux applied) is set to y-axis and y-axis(sensor output voltage) is set to x-axis. After doing his, a 4^{th} order polynomial curve fit is performed. By getting and applying mathematical expression for data points, the sensor response is directly represented as magnetic flux (nT) on the system display and system linear response is increased. The results with this curve fitting based calibration are shown in Figure 4.29 and Figure 4.30 In these figures, the x-axes are applying magnetic fields and y-axes are actual system measurement output read on the system display. The mathematical expression for curve fitted calibartion was programmed in C^{++} program (system.cpp). This microprocessor based signal demodulation system enables to utilize curve fitting based calibration without using complex analog computing circuitry which uses many analog dividers and multipliers. Since the calculations for quadrature signal demodulation and output(magnetic flux) from 4^{th} order fitted curve are done in digital domain, the accuracy of system output was increased.

In Figure 4.29, the first row of the figures is the sensor output voltage corresponding applied calibration magnetic fields. The second row of the figure shows converting the axes, and '*' are converted data points and 'o' are 4^{th} order curve fitted points. This is the first stage of calibration. At this stage, coefficients for mathematical expression are obtained with this method. Figure 4.30 shows the final system calibration curve based on the curve fitting method for x-axis. Even though the sensor output is not linear, the curve fitting based system calibration shows linear output in final representation. The other axes are calibrated by using same method.

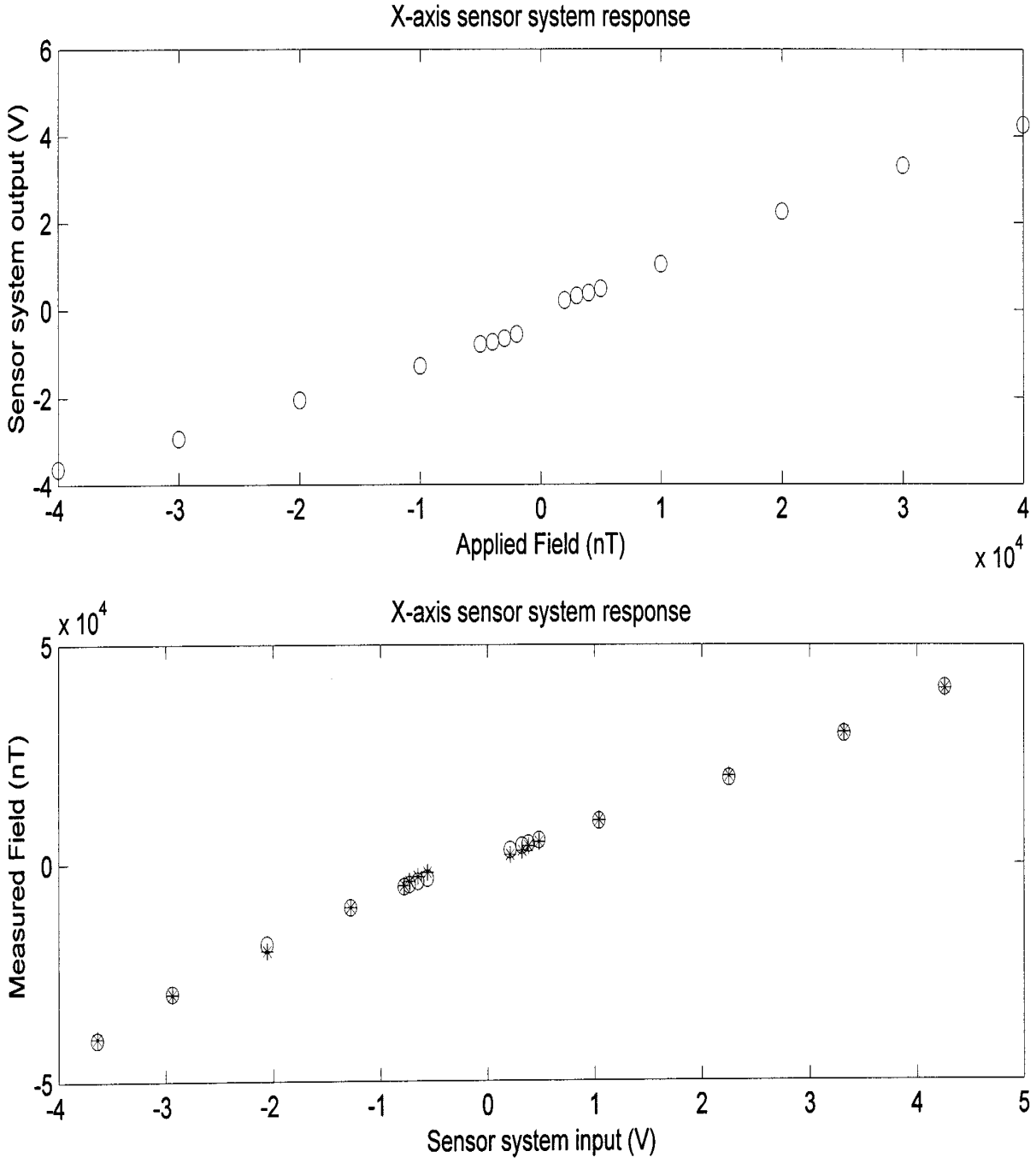

Figure 4.29 First stage of system calibration for X-axis.

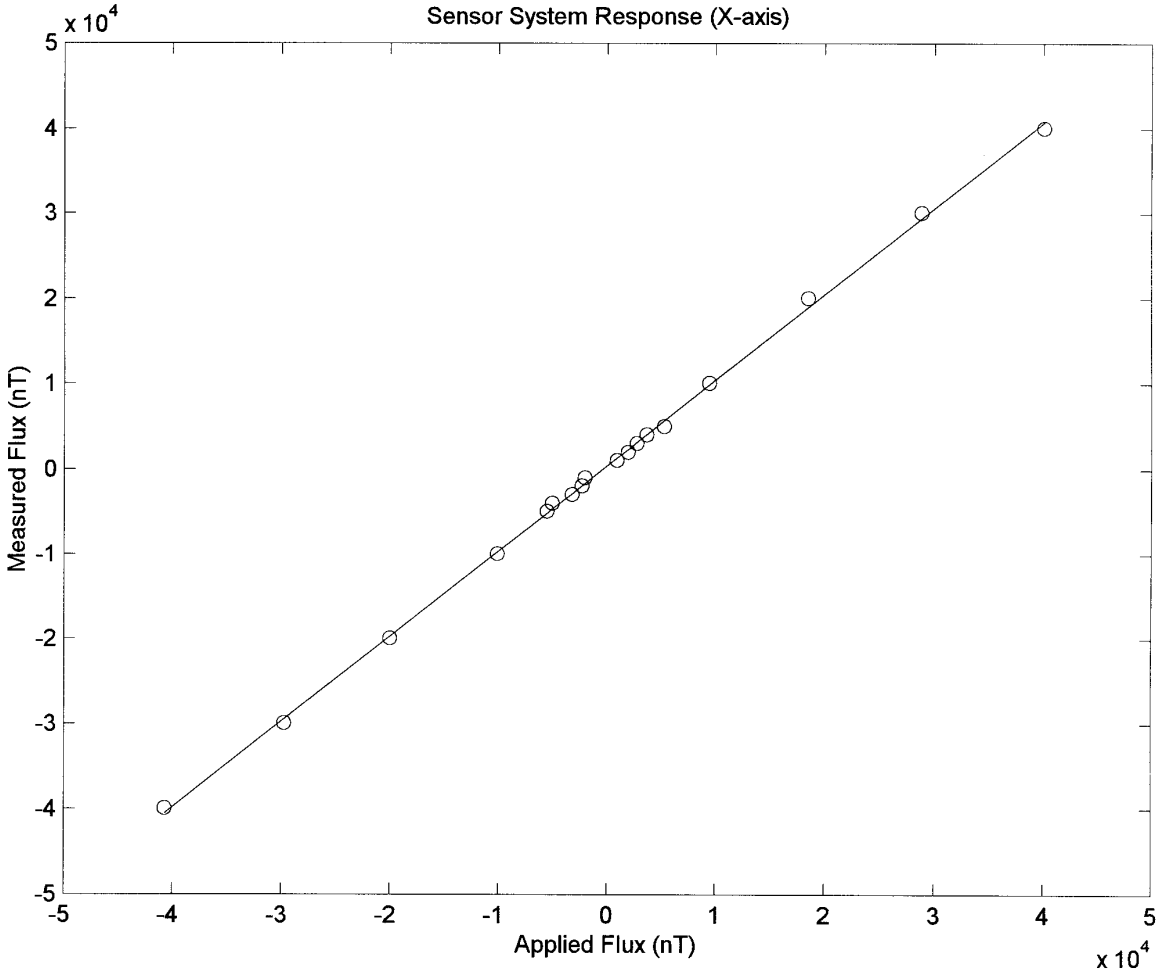

Figure 4.30 Second stage of system calibration for X-axis(final system output representation).